ADVANCED FUNCTIONAL MATERIALS

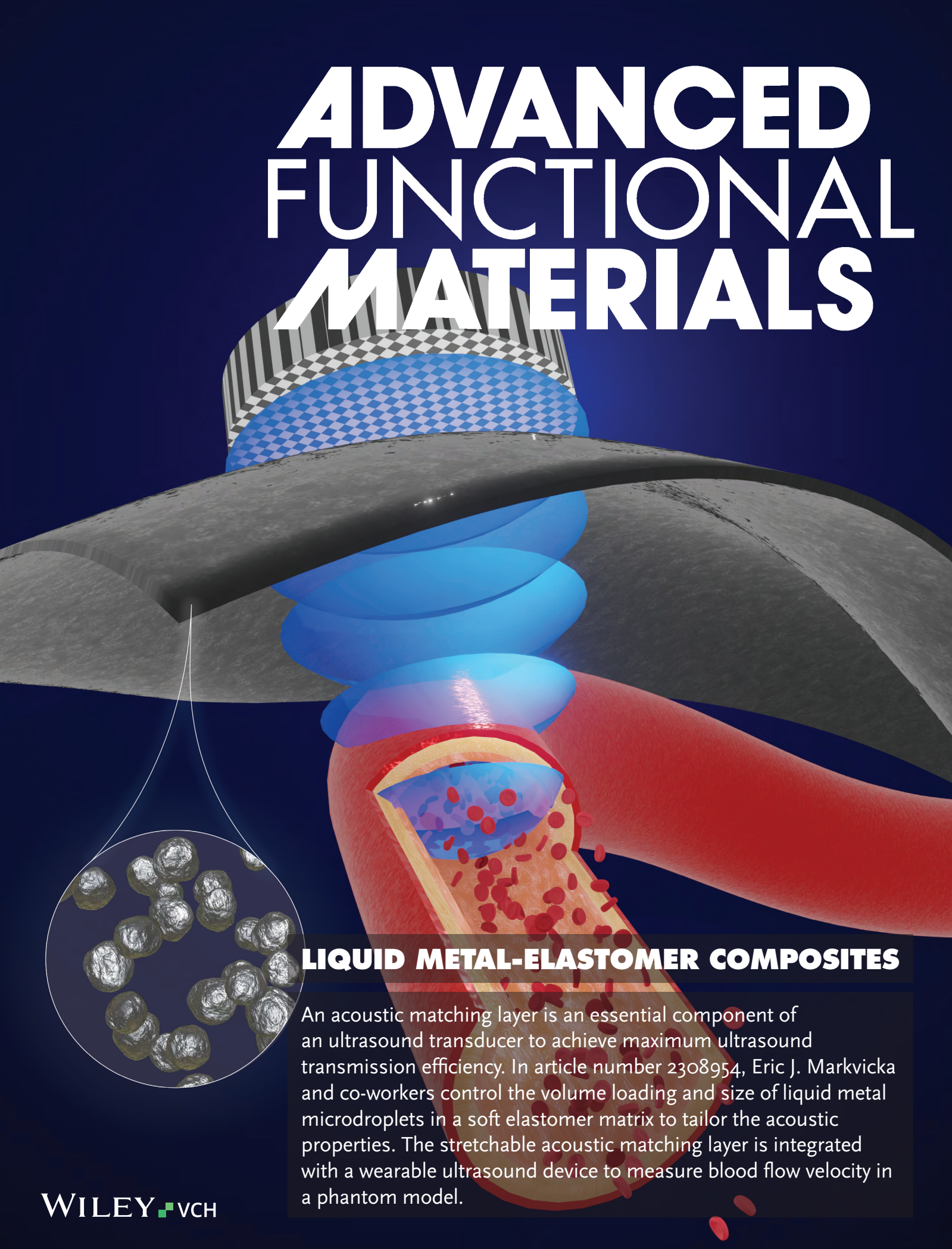

LIQUID METAL-ELASTOMER COMPOSITES

An acoustic matching layer is an essential component of an ultrasound transducer to achieve maximum ultrasound transmission efficiency. In article number 2308954, Eric J. Markvicka and co-workers control the volume loading and size of liquid metal microdroplets in a soft elastomer matrix to tailor the acoustic properties. The stretchable acoustic matching layer is integrated with a wearable ultrasound device to measure blood flow velocity in a phantom model.

WILEY VCH

ADVANCED FUNCTIONAL MATERIALS
www.afm-journal.de

Acoustic Properties of Stretchable Liquid Metal-Elastomer Composites for Matching Layers in Wearable Ultrasonic Transducer Arrays

*Ethan J. Krings, Benjamin D. Hage, Sequoia L. Truong, Kiersten A. Reeser, Eli L. Fox, Matthew G. Snyder, Quentin Walker, Gregory R. Bashford, and Eric J. Markvicka**

Ultrasound is a safe, noninvasive diagnostic technique used to measure internal structures such as tissues, organs, and arterial and venous blood flow. Skin-mounted wearable ultrasound devices can enable long-term continuous monitoring of patients to provide solutions to critical healthcare needs. However, stretchable ultrasound devices that are composed of ultrasonic transducers embedded in an elastomer matrix are incompatible with existing rigid acoustic matching layers, leading to reduced energy transmission and reduced imaging resolution. Here, a systematic study of soft composites with liquid metal (LM) fillers dispersed in elastomers reveals key strategies to tune the acoustic impedance of soft materials. Experiments supported by theoretical models demonstrate that the increase in acoustic impedance is primarily driven by the increase in density with negligible changes to the speed of sound through the material. By controlling the volume loading and particle size of the LM fillers, a material is created that achieves a high acoustic impedance 4.8 Mrayl, (> 440% increase over the polymer matrix) with low modulus (< 1 MPa) and high stretchability (> 100% strain). When the device is mechanically strained, a small decrease is observed in acoustic impedance (< 15%) with negligible decrease in sound transmittance and impact on attenuation for all droplet sizes. The stretchable acoustic matching layer is then integrated with a wearable ultrasound device and the ability to measure motion is demonstrated using a phantom model as is performed in Doppler ultrasound.

1. Introduction

Skin-mounted electronics that mimic the mechanical properties of natural human skin have enabled continuous monitoring of physiological signals.[1–3] However, these devices are limited to physiologic metrics that can be recorded from the surface of the skin such as heart rate,[1,4] skin temperature,[5,6] motion,[7,8] and the presence of specific compounds found in sweat or odors.[9,10] To provide access to deep tissue and organ functions, wearable ultrasound devices have been created consisting of piezoelectric elements embedded in a stretchable substrate.[11–17] These devices provide exciting potential solutions to critical healthcare needs by enabling long-term monitoring of cardiac tissue and arterial and venous blood flow.[17,18] While these devices provide improved wearability compared to conventional ultrasound probes, stretchable ultrasound devices lack matching layers that are essential for optimizing the transmission of ultrasound waves, leading to poor energy transmission into the body and decreased resolution.[19] Matching

E. J. Krings, E. J. Markvicka
Smart Materials and Robotics Laboratory
Department of Mechanical & Materials Engineering
University of Nebraska–Lincoln
Lincoln, NE 68588, USA
E-mail: eric.markvicka@unl.edu

B. D. Hage, E. L. Fox, M. G. Snyder, G. R. Bashford
Biomedical Imaging and Biosignal Analysis Laboratory
Department of Biological Systems Engineering
University of Nebraska–Lincoln
Lincoln, NE 68588, USA

The ORCID identification number(s) for the author(s) of this article can be found under https://doi.org/10.1002/adfm.202308954

DOI: 10.1002/adfm.202308954

S. L. Truong
Department of Biomedical Engineering and Mechanical Engineering
Worcester Polytechnic Institute
Worcester, MA 01609, USA

K. A. Reeser
Department of Biomedical Engineering
LeTourneau University
Longview, TX 75602, USA

Q. Walker
Department of Biomedical Engineering
The Ohio State University
Columbus, OH 43210, USA

E. J. Markvicka
Department of Electrical & Computer Engineering
University of Nebraska–Lincoln
Lincoln, NE 68588, USA

E. J. Markvicka
School of Computing
University of Nebraska–Lincoln
Lincoln, NE 68588, USA

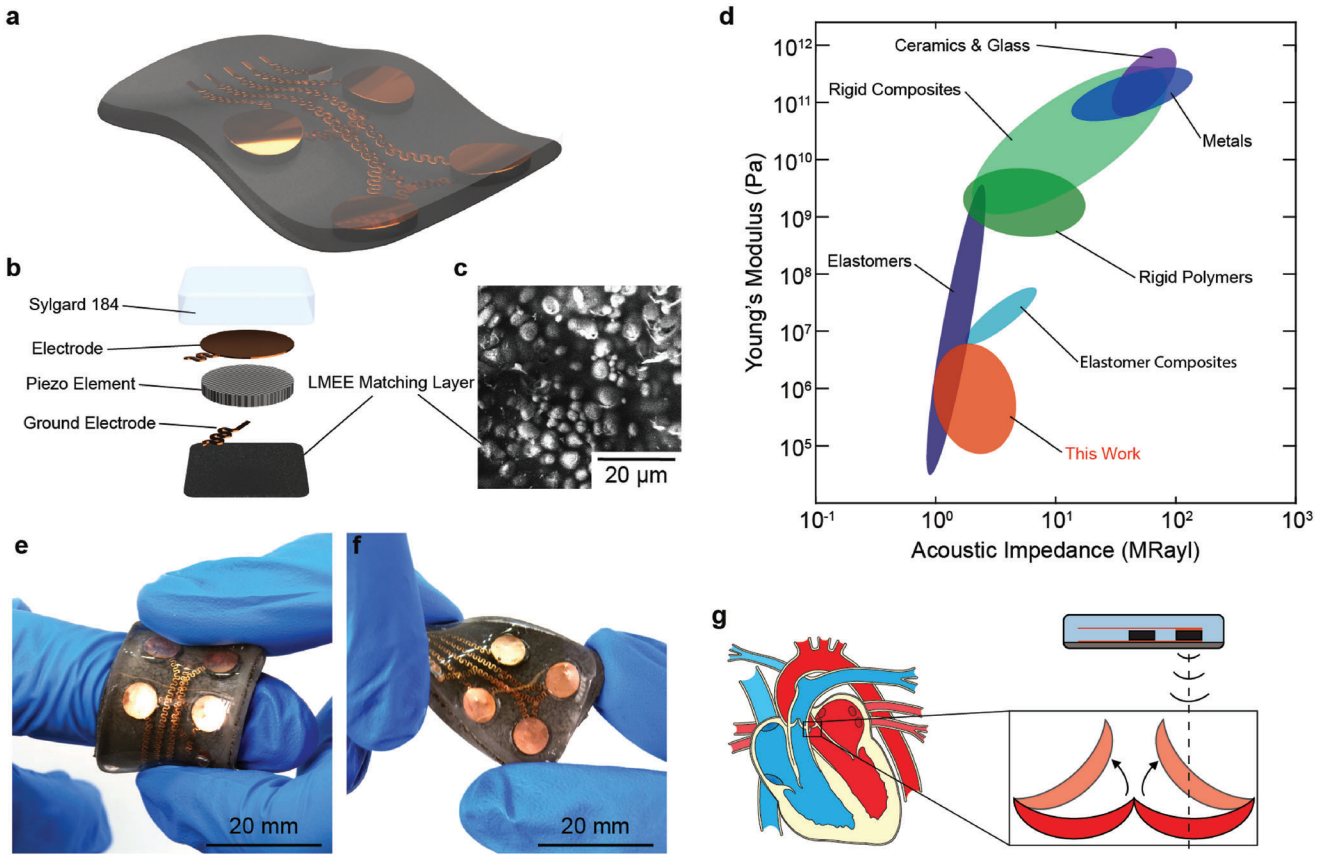

Figure 1. LM-elastomer composites with tunable acoustic impedance. a) Schematic illustration and b) exploded view illustration of a stretchable ultrasonic transducer array with LM-elastomer composite matching layer. c) SEM micrograph of LM droplets embedded in elastomer matrix. d) Plot of Young's modulus versus acoustic impedance for various impedance matching layers. e,f) Photographs of the stretchable ultrasound device with LM-elastomer composite matching layer under deformation. g) Schematic illustration of possible application of the stretchable ultrasound array with matching layer where heart valve motion is continuously monitored (i.e., tissue Doppler).

layers are located between the piezoelectric element and imaging medium to improve sound transmission by reducing losses due to acoustic impedance mismatch.[20] Thus far, matching layers have not been implemented in most wearable ultrasound devices due to the rigid nature of conventional matching layers that are often constructed by doping epoxy with rigid particle fillers.[21–23] Although rigid particles can be incorporated into silicones, urethanes, and acrylate-based elastomers to increase their acoustic impedance,[24–27] the loading required to achieve significant acoustic property enhancement can degrade the mechanical properties of these soft and stretchable material systems.[28–30] Furthermore, the large mismatch in density and elastic modulus between the rigid filler and matrix can cause high attenuation.[24] Alternatively, liquid fillers can be incorporated into elastomers to overcome the inherent mechanical mismatch between the filler and matrix.[31,32] However, liquids typically have a lower density than solids and the speed of sound through liquids is generally lower than through solids, resulting in negligible increases, and even decreases, in acoustic impedance.[26]

Some of the most prominent functional liquid fillers utilized in elastomer composites have been Ga-based liquid metals (LMs), such as eutectic gallium–indium (EGaIn) and Galinstan, which have been engineered to exhibit a wide range of potential properties, including high electrical and thermal conductivity,[33–44] shape-morphing,[45,46] and stiffness tuning.[47,48] These composites are also able to undergo high strain under repeated cyclic loading without loss of mechanical functionality.[33] Ga-based LMs are particularly attractive liquid fillers for an acoustic matching layer due to the high density (ρ_{EGaIn} = 6.25 g·cm^{-3}) as compared to other liquids and to the relatively high speed of sound through the individual components: pure liquid In (c_{In} = 2.320 mm·μs^{-1}) and pure liquid Ga (c_{Ga} = 2.873 mm·μs^{-1}).[49] Previous work has demonstrated that for LM composites with continuous conductive networks, the LM filler acts as an effective electromagnetic shield over a broad frequency range (3–40 GHz).[50,51] However, there are limited studies at lower frequency ranges that are appropriate for ultrasound imaging (2–20 MHz) with electronically insulating composites with discrete droplets. Furthermore, no report has been made on the speed of sound through Ga-based LM alloys.

Here, we introduce the fabrication, characterization, and use of an LM elastomer composite with tunable acoustic properties for use as a matching layer in stretchable ultrasonic transducer arrays (**Figure 1**a–c). By combining recent work on LM elastomer composites and wearable ultrasound devices, the incorporation of a liquid phase into elastomers eliminates the mechanical

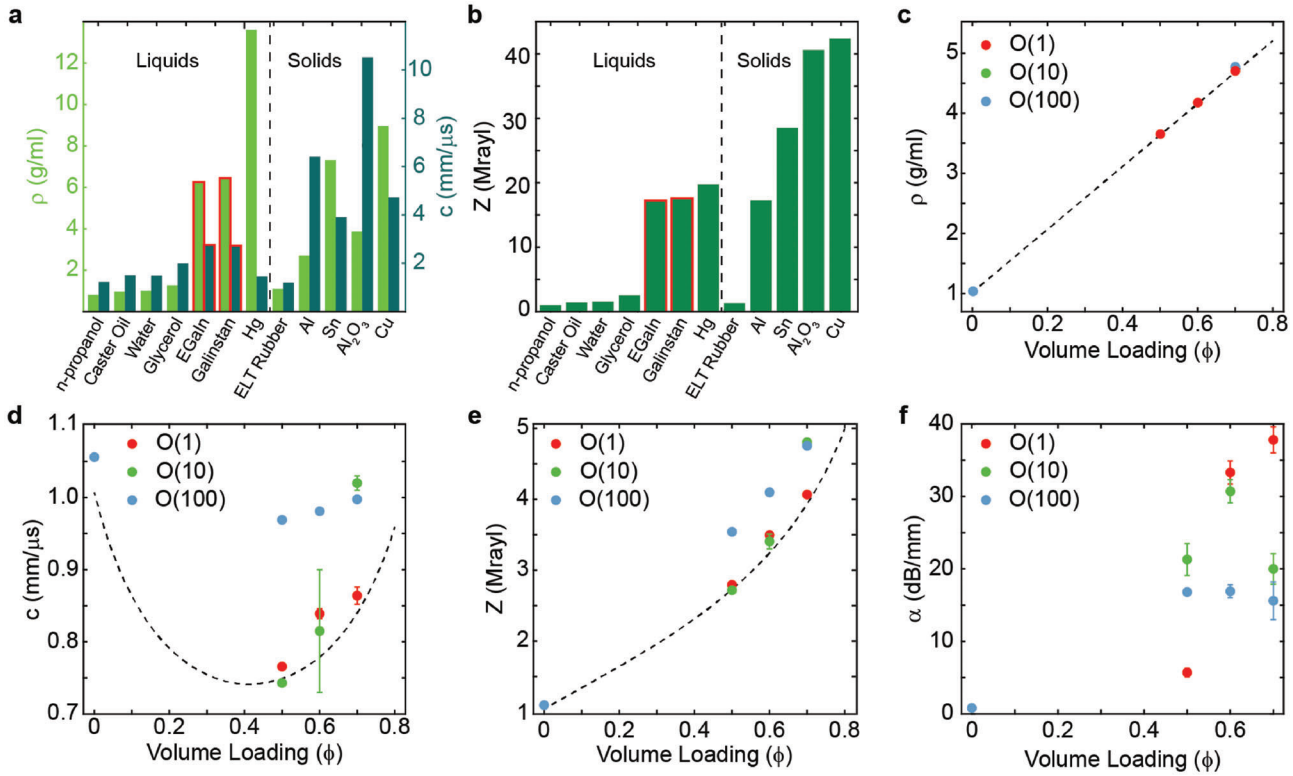

Figure 2. LM and LM-elastomer composite acoustic properties. a) Density, speed of sound, and b) acoustic impedance of EGaIn and Galinstan compared to other materials used in polymers to tune the acoustic impedance. c) Density, d) speed of sound, e) acoustic impedance, and f) attenuation of LM-elastomer composite with O(1), O(10), and O(100) LM droplet diameters at different volume loadings (ϕ = 0, 0.5, 0.6, 0.7). c) Dashed line is the predicted density. d) Dashed line is predicted speed of sound from the Wood's model. e) Dashed line is predicted impedance from predicted density and sound speed from the Wood's model. All error bars represent ±1 SD and are not displayed if smaller than the data point size. $n = 3$ samples were tested for all data points.

compliance mismatch of rigid fillers and thus preserves the mechanics of the host elastomer, offering a unique combination of low stiffness and high acoustic impedance. The integration of LM microdroplets increases the acoustic impedance to over 440%, displays a low attenuation, and maintains a soft and stretchable response (Figure 1d–f). The LM-based acoustic matching layer can be integrated with an array of individually addressable ultrasonic transducers (Figure 1e,f). As illustrated in Figure 1g, the ultrasound device can be used to detect the motion of deep tissue and organ functions such as the motion of heart valves and ventricle walls,[17,52] which was demonstrated using an ultrasound phantom model.

2. Results and Discussion

2.1. Acoustic Impedance of LM

The acoustic impedance of a material can be calculated by multiplying the density of the material by the speed of sound of through the material: $Z = \rho \cdot c$, where Z is acoustic impedance, ρ is material density, and c is speed of sound. We selected Ga-based LM such as EGaIn (75% Ga and 25% In by weight) and Galinstan (68.5% Ga, 21.5% In, and 10% Sn by weight) as the liquid filler for the acoustic matching layer due to its combination of high density (6.25 and 6.44 g·cm^{-3}, respectively), low viscosity, and non-toxic characteristics.[53,54] The speed of sound through the room temperature LM was measured in water using a transmission-through method where the LM was placed in a glass cuvette between two ultrasonic transducers, one configured as an emitter, and one configured as a receiver (Figure S1, Supporting Information). The speed of sound through EGaIn was determined to be 2.753 ± 0.005 mm· μs^{-1} (**Figure 2**a), which falls between the previously recorded speeds of sound through pure liquid indium (2.320 mm· μs^{-1}) and liquid gallium (2.873 mm· μs^{-1}) at their respective melting temperatures.[49] The acoustic impedance of Galinstan was 2.730 ± 0.003 mm· μs^{-1}. In comparison to other liquids previously used for impedance matching layers, both the density and speed of sound through EGaIn and Galistan are significantly higher (Figure 2a), resulting in higher acoustic impedances of Z = 17.21 Mrayl and Z = 17.58 MRayl, respectively (Figure 2b).[55–57] The acoustic impedances for EGaIn and Galinstan are comparable to aluminum (Al) particles (Z = 17.28 Mrayl), but are lower than other metals and metal oxides often used in impedance matching layers, such as cerium dioxide or aluminum oxide with acoustic impedance > 40 Mrayl.[25,27,55,58] Mercury (Z = 19.58 Mrayl) is the only other liquid with an impedance comparable to EGaIn and Galinstan; however, its high toxicity makes it unsuitable for wearable applications.

2.2. Acoustic Impedance of LM-Elastomer Composites

To enable integration with stretchable ultrasound devices, EGaIn was dispersed as microdroplets in a soft silicone elastomer (Sylgard 184; Dow Corning), as previously described.[35,44] To understand the effects of the LM inclusions on the acoustic properties of the silicone elastomer, the volume loading (ϕ = 50 to 70%) and diameter of the LM microdroplets were varied. Three different droplet size scales were chosen with diameters on the order of 100 µm (O(100)), 10 µm (O(10)), and 1 µm (O(1)). The LM composites with O(10) and O(100) LM droplets were fabricated by shear mixing bulk EGaIn with the silicone prepolymer using a planetary mixer. The low viscosity of the prepolymer prevented the formation of O(1) droplets with the planetary mixer, so an alternative emulsion shearing method was used where O(1) LM droplets were formed by shear mixing bulk EGaIn in an acetic acid solution.[59] The droplets were washed, dried, and then dispersed into the prepolymer. The droplet size and distribution were confirmed using a combination of optical microscopy (AXIO Zoom.V26, Zeiss) and scanning electron microscope (FEI Helios NanoLab 660) imaging (Figure S2a–c, Supporting Information). ImageJ was used to determine average particle diameter and size distribution (Figure S2d–f, Supporting Information). The O(100), O(10), and O(1) LM droplets had mean diameters of 190 µm ($\pm$ 59.4 µm), 37.1 µm ($\pm$ 13.2 µm), and 3.79 µm ($\pm$ 1.24 µm), respectively. To ensure consistent and uniform thickness with minimal surface roughness, independent of LM volume loading and LM droplet size, which can influence the viscosity of the emulsion, the samples were compression molded and cured in a pressure pot (Figure S3, Supporting Information).

The densities of the LM-elastomer composites were measured gravimetrically using a density determination kit (80253384, Ohaus). As expected, we saw a linear increase in density as the volume loading of LM was increased from 50% to 70% by volume for all LM droplet sizes (Figure 2c). These experimental results closely match the theoretical density $\rho_{LME} = \phi \cdot \rho_{LM} + (1 - \phi) \cdot \rho_{matrix}$, where $\phi = \frac{vol(LM)}{vol(LM+matrix)}$ is the volume fraction of LM, and ρ_{LM} and ρ_{matrix} is the density of the LM and silicone elastomer, respectively. These results indicate that no air voids were introduced into the composite during fabrication.

The speed of sound through the composite was measured using a transmission-through method where the sample was attached to a frame and placed between two ultrasonic transducers immersed in water (Figure S4, Supporting Information). A pulse was sent through the sample of known thickness (1 mm) and was received by another immersed transducer. The signal was sampled using a digital oscilloscope, and the speed of sound through the material was calculated (see Supporting Information for additional details). As shown in Figure 2d, the speed of sound through the unfilled silicone was observed to have the highest speed of sound as compared to any of the LM composites (ϕ = 50% to 70%) tested. For the LM-elastomer composite, the speed of sound increased with increasing volume loading of LM from 50 to 70% for all droplet sizes, which can be predicted by the Wood's model:[60,61]

$$c_{wood} = \frac{1}{\sqrt{[(1-\phi)\rho_m + \phi\rho_f] \cdot [(1-\phi)\chi_m + \phi\chi_f]}} \quad (1)$$

where ρ_f and χ_f are the density and compressibility of the LM filler and ρ_m and χ_m are the density and compressibility of the elastomer matrix. The O(1) and O(10) diameter particles show reasonable agreement with the model. However, as the particles increase in size O(100), a sharp increase in the speed of sound is observed. For all conditions tested, we do not expect the formation of cavitation induced LM particle networks, as previously observed using probe sonication.[62] The acoustic energy generated by the piezoelectric transducers (0.72 W·cm^{-2}) is significantly lower than the acoustic energy used to induce LM particle networks generated by probe sonication (194.5 W·cm^{-2}).

The acoustic impedance of the LM composite was then determined. For the LM-elastomer composite, the acoustic impedance monotonically increased with increasing LM volume loading for all LM droplet sizes with ϕ = 70% samples increasing to over 400% as compared to the unfilled silicone for all droplet sizes (Figure 2e). The increase in acoustic impedance is primarily driven by the increase in density with negligible decreases to the speed of sound through the composite. As observed with the speed of sound measurements, the acoustic impedance generally increases with LM droplet size.

Signal attenuation is another important factor to consider when designing acoustic matching layers. A matching layer with high attenuation will drastically reduce the amplitude of the sound waves before they are able to propagate into the skin. Factors such as inclusion shape, size, and relative impedance can affect the attenuation of particle-filled composites.[24] In this work, we characterized the effect of particle size and volume loading on attenuation in LM-elastomer composites as shown in Figure 2f. The attenuation of the O(1), ϕ = 0.5 composite was the lowest recorded for all LM samples (5.7 dB·mm^{-1}). The attenuation increased substantially to 33.3 dB·mm^{-1} and 37.8 dB·mm^{-1} for ϕ = 0.6 and 0.7, which were the most attenuating of all samples tested. The O(100) samples had the least variation in attenuation with all volume loadings in the 15 to 17 dB·mm^{-1} range.

2.3. Acoustic-Mechanical Characterization

A matching layer integrated into a stretchable ultrasound device would undergo elastic deformation perpendicular to the direction of sound wave propagation (**Figure 3**a inset). In contrast to rigid particle fillers, the shape of liquid phase fillers can be controlled through the application of strain, which can significantly impact thermal conductivity[33] with negligible changes to electrical conductivity.[44] Here, we examined the acoustic properties of the LM-elastomer matching layer as a function of strain and LM droplet shape for the three different droplet diameters at a constant volume loading ϕ = 0.5. The LM-elastomer composites were strained to 20% and 40% and the acoustic impedance and attenuation were measured at each strain value as previously described (Figure S5, Supporting Information). Figure 3a shows that the impedance for all three droplet sizes decreased as the axial strain increased from 0% to 40%. The impedance of the O(1) and O(100) composites remained relatively unchanged as the samples were strained from 0% to 40% while the impedance of the O(10) composite decreased by 13%. The solid black line in Figure 3b indicates the theoretical sound intensity transmitted into the skin for a matching layer with the corresponding

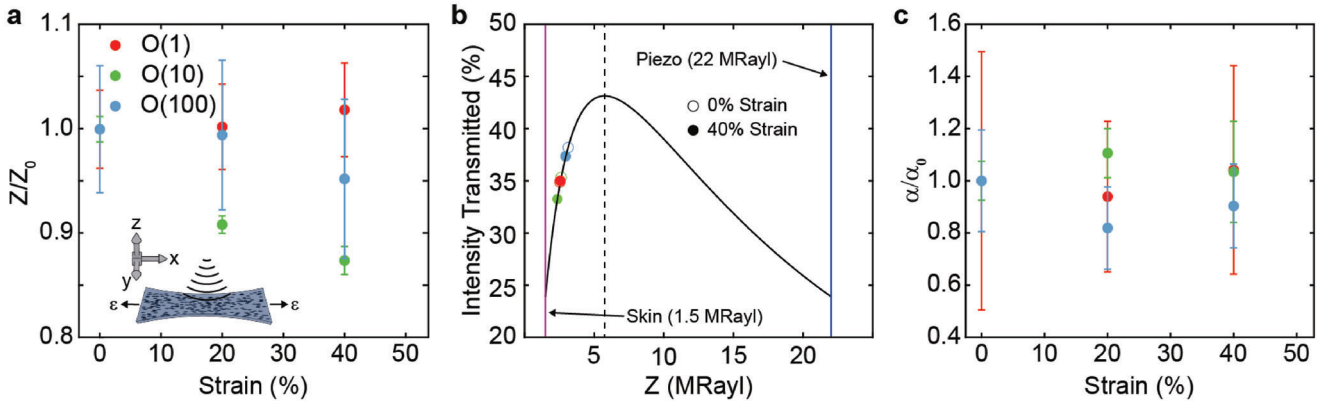

Figure 3. LM-elastomer composite acoustic properties as a function of strain. a) Relative impedance of the LM-elastomer composite with O(1), O(10), and O(100) LM droplet diameters under axial strain for $\phi = 0.5$. b) Theoretical sound intensity transmitted through matching layer based on matching layer impedance (black line). Markers indicate theoretical transmittance of O(1), O(10), and O(100) LM matching layers ($\phi = 0.5$) based on the measured impedance from (a). Dashed line indicates optimal matching layer impedance. Magenta and dark blue lines indicate the skin and piezoelectric transducer impedance, respectively. c) Relative attenuation of the LM-elastomer composite with O(1), O(10), and O(100) LM droplet diameters as a function ofaxial strain for $\phi = 0.5$. All error bars represent ±1 SD and are not displayed if smaller than the data point size. $n = 3$ samples were tested for all data points.

acoustic impedance on the x-axis and piezoelectric element with an acoustic impedance of 22 Mrayl. The O(1) LM-elastomer composite sample had a theoretical transmitted sound intensity of 35.5% while unstretched that decreased to 35% as the sample was stretched to 40% strain. The O(10) LM-elastomer composite had an unstretched sound transmittance of 36% that decreased to 33% transmittance at 40% strain. The O(100) had the highest theoretical transmittance of 37% intensity at 0% strain. The decrease in impedance as the sample was strained to 40% resulted in a 1.5% decrease in transmitted sound intensity. The drop in impedance and consequent loss in sound transmittance was negligible for $\phi = 0.5$ for all droplet sizes. The attenuation of the O(1) composite remained approximately constant as the samples were strained, the attenuation of the O(10) composite increased by a maximum of 10% of the initial attenuation under 20% strain, and the attenuation of the O(100) composites decreased by a maximum of 20% of the initial attenuation under 20% strain (Figure 3c). The change in LM droplet shape due to the deformation of the matching layer therefore had only a small impact on attenuation at strain values typically seen in wearable devices (< 30%).

2.4. Wearable Ultrasound Device with LM-Elastomer Matching Layer

A stretchable, wearable ultrasound patch with a 2 × 2 piezoelectric element array and stretchable LM-elastomer matching layer was fabricated (Figure 1). The piezoelectric elements (1-3 Composite, PZT Navy Type II 5A, Smart Material Corp., Sarasota, FL) contained randomly arranged fibers with fiber diameter of 250 μm and 65% fill. The elements had a diameter of 6 mm and a measured center frequency of 2.75 MHz. The optimal acoustic impedance of the matching layer was determined to be 5.74 Mrayl from $Z_m = \sqrt{Z_1 \cdot Z_2}$, where Z_1 and Z_2 are the acoustic impedances of the piezoelectric elements (22 Mrayl) and skin (1.5 Mrayl), respectively. The ideal thickness of the matching layer is equal to 1/4 of the length of the acoustic wave (λ) traveling through the layer to minimize wave reflection.[63] Using the Wood's model (Equation 1) to calculate speed of sound through the LM-elastomer composite, the quarter wavelength ($\lambda/4$) matching layer thicknesses were determined to be 89, 97, and 100 μm for ϕ = 0.5, 0.6, and 0.7 LM volume loadings, respectively. The relatively thin (<100 μm) $\lambda/4$ matching layer led to only the O(1) LM-elastomer composite being viable for fabrication. The high attenuation (<30 dB·mm^{-1}) of the $\phi = 0.6$ and 0.7 LM volume loadings led to the selection of the $\phi = 0.5$ LM volume loading.

An A-line from the wearable ultrasound device with LM-elastomer acoustic matching layer is shown in **Figure 4**a. We observe a short A-line pulse duration (about four cycles at 2 MHz), which is desired for good axial resolution in diagnostic medical ultrasound imaging.[20] In contrast to other modes of diagnostic ultrasound imaging, in which a low number of pulses are desired for high axial resolution, Doppler ultrasound typically employs pulses with durations of 10–50 cycles.[64,65] Accordingly, a 50 V amplitude, two-level pulse with a 10-cycle duration was used to excite the piezoelectric transducers (Figure 4b, top). The resulting acoustic output was measured using a hydrophone placed 26 mm away from the device (Figure 4b, bottom). This acoustic output illustrates the lowpass filter effect of the piezoelectric transducers, and confirms that the device can send and receive pulses similar to those used in Doppler ultrasound. Sensitivity was computed for two individual piezo elements, giving values of 122 and 129 dB re 1 µPa/V @ 1 m.

The device was then used to detect motion, as would be performed in Doppler ultrasound, using a phantom model. Doppler ultrasound can be used to detect motion of deep tissue such as heart valves and ventricle walls,[17] as well as the flow of blood.[18] A phantom model was created for motion detection (Figure 4c,d). The phantom model consisted of a ruler that was moved away from the device at a constant rate of approximately 3.8 cm·s^{-1}. A piece of sandpaper (3M Pro Grade 100-grit, 3M, St. Paul, MN) was affixed to the ruler to simulate scatterers such as red blood cells. Figure 4e shows the resulting A-lines when the ruler was moved away from the device at a constant velocity. The sloping

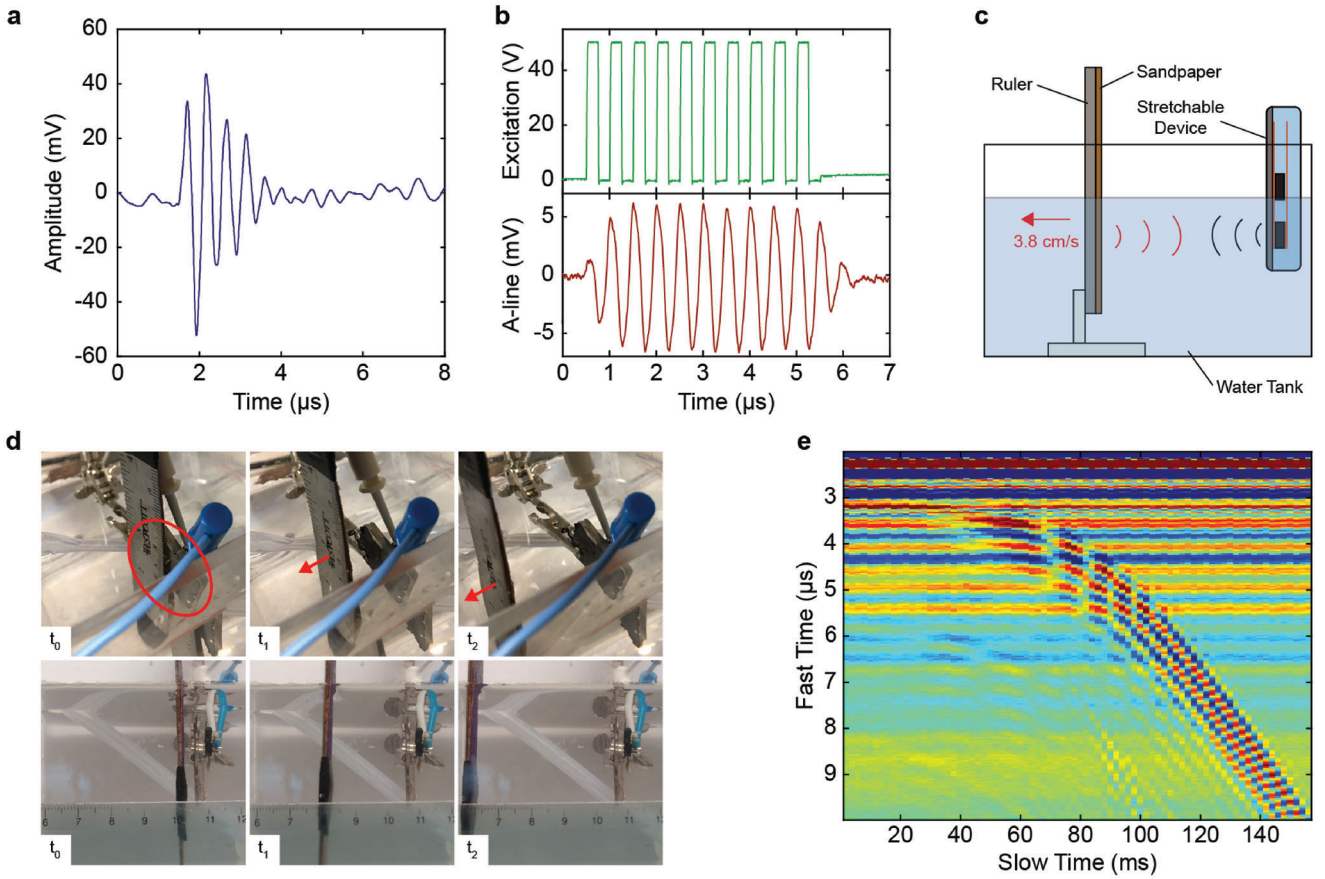

Figure 4. Demonstration of a stretchable ultrasound device with acoustic matching layer. a) A-line from the 2×2 piezoelectric element array. The target was a flat aluminum block. b) Top: two-level excitation pulse with 10 cycles at a frequency of 2 MHz, which is commonly used in a Doppler ultrasound device. Bottom: Shape of the resultant acoustic output, measured by a hydrophone placed 26 mm from the device. c) Schematic illustration and d) photograph of the phantom model for detection of motion with the ultrasound device. The ultrasound device is circled and the direction of motion is shown by the red arrow. e) A-lines (each column is one A-line) illustrating motion away from the device at approximately 3.8 $cm \cdot s^{-1}$.

lines represent motion away from the device and are caused by the increasing round-trip time for each successive sound pulse. The set of consecutive A-lines can be used to calculate the velocity of motion or flow toward or away from a transducer as a function of time.[18]

3. Conclusion

Acoustic matching layers are typically composed of rigid particles embedded in a polymer matrix, which limits their use in stretchable ultrasound devices. In this work, we describe and demonstrate a soft and stretchable acoustic matching layer that was created by embedding LM inclusions within a soft elastomer matrix. The relatively high density (6.25 $g \cdot cm^{-3}$) and fluidity of the room-temperature LM allows for the fabrication of soft composites with acoustic impedance as high as 4.8 Mrayl, which represents >440% increase in acoustic impedance as compared to the unfilled elastomer. However, the LM inclusions do increase the attenuation of the ultrasound signal, especially for the O(1) LM droplets. Under strains typically observed in wearable devices, we observed negligible changes to transmitted sound or attenuation. The performance of the acoustic matching layer could be further improved by functionalizing the surface of the LM droplets to improve the size distribution and interface between the polymer matrix[66] or considering LM mixtures with high impedance particles.

4. Experimental Section

LM-elastomer Composite Fabrication: The O(10) and O(100) droplet diameter LM-elastomer composite matching layers were fabricated by shear mixing bulk EGaIn with the uncured prepolymer using a Flacktek planetary mixer. The cross-linker was then added to the LM/prepolymer mixture at a 10:1 prepolymer to cross-linker mass ratio and mixed for an additional minute at the lowest speed setting. The O(1) LM droplets were first fabricated using the SLICE method[59] by shear mixing bulk EGaIn in 5% acetic acid at a 20:1 acetic acid to EGaIn volume ratio. The droplets were formed by mixing 20 min at 20000 RPM with a Dremel rotary tool and custom-printed mixer attachment. The LM microdroplets were allowed to sediment, and the acetic acid was decanted. Ethanol was added to the LM microdroplets to rinse off any excess acetic acid, and the mixture was again allowed to sediment and decanted. The LM microdroplets were placed in a 70°C convection oven to evaporate any remaining ethanol. After the microdroplets had cooled to room temperature, they were combined with the prepolymer and mixed in the Flacktek mixer for 1 min at the lowest

speed setting. The cross-linker was added at a 10:1 prepolymer to cross-linker mass ratio, and the uncured composite was mixed again for 1 min at the lowest setting. The uncured composites were poured into a custom-made compression mold that was bolted together to form the matching layer shape. The mold was placed in a pressure pot at 40 psi and 70°C for 8 h to prevent the formation of air pockets in the cured composite. Hexane was added to the prepolymer due to the high viscosity of the uncured 70 vol.% LM, O(1) droplet diameter mixture. Hexane was added to the prepolymer at a 10:1 prepolymer to hexane ratio, mixed (both mixing steps), and then evaporated under vacuum for 1 h before the uncured elastomer was poured into the mold.

Speed of Sound Measurements: The speed of sound was measured using a pitch-catch experiment with a 2.25 MHz unfocused immersion transducer (0.5 inch diameter, IR-0208-S, Harisonic) as the emitter, and a 3.5 MHz unfocused immersion transducer (0.5 inch diameter, IR-0308-S, Harisonic) as the receiver. The speed of sound of pure EGaIn was measured by placing the EGaIn in a glass cuvette and placing the cuvette in water between the two transducers. The speed of sound of LM-elastomer composite samples was measured by placing the LM-elastomer composite samples in water between the two transducers (see Supporting Information for more details).

Acoustic Attenuation Measurements: Acoustic attenuation was measured with the same setup that was used for measuring speed of sound (see Supporting Information for more details).

Stretched Samples: Speed of sound measurements and acoustic attenuation measurements were repeated for LM-elastomer composites containing 50% LM with (O(1)), (O(10)), and (O(100)) droplet sizes. All measurements were made as described for unstretched samples. A custom frame (Figure S5, Supporting Information) was made to hold samples at strains of up to 40%. Measurements were made at 0%, 20%, and 40% strain. Sample thicknesses were measured at each strain level to ensure accuracy in the speed of sound calculation.

Density Measurements: Density measurements of the LM-elastomer composites were conducted gravimetrically with a density determination kit (80253384, Ohaus). The mass of each composite sample was measured in air and recorded. The sample placed in ethanol and the mass of the sample was again recorded. The temperature of the ethanol was recorded to determine the ethanol density using tables provided with the density determination kit.

Wearable Ultrasound Device Fabrication: The stretchable ultrasound device was fabricated using a series of compression and injection molds (Figure S6a-i, Supporting Information). The uncured O(1) LM-elastomer composite with a $\phi = 0.5$ volume loading was prepared using the methods described above and poured into a compression mold made of acrylic upper and lower sections with a 3 mil (76.2 mm) stainless steel spacer providing the $\lambda/4$ thickness. The mold was bolted shut to apply compression. The matching layer was then cured at 70°C for 8 h under 40 psi to prevent the expansion of any potential air voids in the LM-elastomer composite. The matching layer mold was cooled, and the top half of the acrylic compression mold was removed. The copper ground electrode was placed on the matching layer, and the piezoelectric elements were mounted to the electrode with silver conductive epoxy (8331D, MG Chemicals). An acrylic mold was then placed on top of the matching layer and electrodes, and uncured Sylgard 184 was injected into the mold and cured at 80°C for 1 h. The mold was cooled, and the acrylic upper was removed. The top electrodes were fastened to the piezoelectric elements with silver epoxy. A final acrylic mold was placed on top of the unfinished device and additional Sylgard 184 was injected to encapsulate the top electrodes. The mold was cured at 80°C for 1 h and cooled before the completed ultrasound device was removed.

Wearable Ultrasound Demonstration: For generating the A-line shown in Figure 4, the setup was as follows. A piezo element was excited by a very brief (approximately 100 ns) and very high-voltage (approximately 500 V) pulse using a Panametrics 5072PR pulser. The pulse emitted by the piezo was reflected off an aluminum block placed 15 mm from the device, and the returned echo was detected by the piezo and sent to an oscilloscope for measurement.

For generating the acoustic output shown in Figure 4b, a 50 V amplitude, two-level pulse with a 10-cycle duration was used to excite the piezo (Figure 4b, top). The pulse was generated by a Texas Instruments TX517 integrated circuit on an evaluation module (TX517EVM, Texas Instruments, Dallas, TX). The resulting acoustic output was measured using a hydrophone (Onda HGL-0200, Onda Corporation, Sunnyvale, CA) placed 26 mm away from the device (Figure 4b, bottom). Transmitting sensitivity was calculated from the resulting according to established methods,[67] as explained in Supporting Information.

Supporting Information

Supporting Information is available from the Wiley Online Library or from the author.

Acknowledgements

The authors would like to thank Megan Santamore for help with measuring the speed of sound measurements. The authors acknowledge support through the NSF (No. EEC-2050587). S.T., E.K., and E.M. also acknowledge support through the NSF (No. CMMI-2054411) and the Nebraska Tobacco Settlement Biomedical Research Development Fund. E.K. and E.M. also acknowledge support from the NASA Nebraska Space Grant (80NSSC19M0065). The research was performed in part in the Nebraska Nanoscale Facility: National Nanotechnology Coordinated Infrastructure and the Nebraska Center for Materials and Nanoscience, which are supported by the National Science Foundation under Award ECCS: 1542182, and the Nebraska Research Initiative. Manufacturing and characterization analysis were performed at the NanoEngineering Research Core Facility (NERCF), which is partially funded by the Nebraska Research Initiative.

Conflict of Interest

The authors declare no conflict of interest.

Data Availability Statement

The data that support the findings of this study are available from the corresponding author upon reasonable request.

Keywords

acoustic impedance, liquid metals, soft materials, ultrasound, wearable electronics

Received: July 31, 2023
Revised: September 13, 2023
Published online:

[1] D.-H. Kim, N. Lu, R. Ma, Y.-S. Kim, R.-H. Kim, S. Wang, J. Wu, S. M. Won, H. Tao, A. Islam, K. J. Yu, T.-i. Kim, R. Chowdhury, M. Ying, L. Xu, M. Li, H.-J. Chung, H. Keum, M. McCormick, P. Liu, Y.-W. Zhang, F. G. Omenetto, Y. Huang, T. Coleman, J. A. Rogers, *Science* **2011**, *333*, 838.

[2] E. Markvicka, G. Wang, Y.-C. Lee, G. Laput, C. Majidi, L. Yao, in *Proc. of the 2019 CHI Conf. on Human Factors in Computing Systems*, ACM Digital Library, New York, USA **2019**, pp. 1–10.

[3] M. D. Bartlett, E. J. Markvicka, C. Majidi, *Adv. Funct. Mater.* **2016**, *26*, 8496.
[4] J. Alberto, C. Leal, C. Fernandes, P. A. Lopes, H. Paisana, A. T. de Almeida, M. Tavakoli, *Sci. Rep.* **2020**, *10*, 15539.
[5] Y. Yamamoto, D. Yamamoto, M. Takada, H. Naito, T. Arie, S. Akita, K. Takei, *Adv. Healthc. Mater.* **2017**, *6*, 1700495.
[6] S. Han, J. Kim, S. M. Won, Y. Ma, D. Kang, Z. Xie, K.-T. Lee, H. U. Chung, A. Banks, S. Min, S. Y. Heo, C. R. Davies, J. W. Lee, C.-H. Lee, B. H. Kim, K. Li, Y. Zhou, C. Wei, X. Feng, Y. Huang, J. A. Rogers, *Sci. Transl. Med.* **2018**, *10*, eaan4950.
[7] Y. Jin, C. M. Glover, H. Cho, O. A. Araromi, M. A. Graule, N. Li, R. J. Wood, C. J. Walsh, in *2020 IEEE Int. Conf. on Robotics and Automation (ICRA)*, IEEE, Piscataway, NJ **2020**, pp. 4863.
[8] M. McManigal, R. Wilson, P. McManigal, B. Beran, E. Wellsandt, E. J. Markvicka, in *Frontiers in Biomedical Devices*, Vol. *84815*, American Society of Mechanical Engineers, Minneapolis, MN, **2022**, V001T04A002.
[9] J. Finnegan, B. Peterkin, H.-C. Han, J. M. Yentes, S. I. Rennard, E. J. Markvicka, in *Frontiers in Biomedical Devices*, Vol. *84815*, American Society of Mechanical Engineers, Minneapolis, MN **2022**, V001T04A005.
[10] W. Gao, S. Emaminejad, H. Y. Y. Nyein, S. Challa, K. Chen, A. Peck, H. M. Fahad, H. Ota, H. Shiraki, D. Kiriya, D.-H. Lien, G. A. Brooks, R. W. Davis, A. Javey, *Nature* **2016**, *529*, 509.
[11] H. Hu, H. Huang, M. Li, X. Gao, L. Yin, R. Qi, R. S. Wu, X. Chen, Y. Ma, K. Shi, C. Li, T. M. Maus, B. Huang, C. Lu, M. Lin, S. Zhou, Z. Lou, Y. Gu, Y. Chen, Y. Lei, X. Wang, R. Wang, W. Yue, X. Yang, Y. Bian, J. Mu, G. Park, S. Xiang, S. Cai, P. W. Corey, et al., *Nature* **2023**, *613*, 667.
[12] M. Lin, Z. Zhang, X. Gao, Y. Bian, R. S. Wu, G. Park, Z. Lou, Z. Zhang, X. Xu, X. Chen, A. Kang, X. Yang, W. Yue, L. Yin, C. Wang, B. Qi, S. Zhou, H. Hu, H. Huang, M. Li, Y. Gu, J. Mu, A. Yang, A. Yaghi, Y. Chen, Y. Lei, C. Lu, R. Wang, J. Wang, S. Xiang, et al., *Nat. Biotechnol.* **2023**, 1.
[13] W. Liu, C. Zhu, D. Wu, *IEEE Electron Device Lett.* **2021**, *42*, 240.
[14] F. Wang, P. Jin, Y. Feng, J. Fu, P. Wang, X. Liu, Y. Zhang, Y. Ma, Y. Yang, A. Yang, X. Feng, *Sci. Adv.* **2021**, *7*, eabi9283.
[15] C. Wang, X. Li, H. Hu, L. Zhang, Z. Huang, M. Lin, Z. Zhang, Z. Yin, B. Huang, H. Gong, S. Bhaskaran, Y. Gu, M. Makihata, Y. Guo, Y. Lei, Y. Chen, C. Wang, Y. Li, T. Zhang, Z. Chen, A. P. Pisano, L. Zhang, Q. Zhou, S. Xu, *Nat. Biomed. Eng.* **2018**, *2*, 687.
[16] J.-m. S. Kenny, C. E. Munding, J. K. Eibl, A. M. Eibl, B. F. Long, A. Boyes, J. Yin, P. Verrecchia, M. Parrotta, R. Gatzke, P. A. Magnin, P. N. Burns, F. S. Foster, C. E. M. Demore, *Sci. Rep.* **2021**, *11*, 7780.
[17] C. Wang, B. Qi, M. Lin, Z. Zhang, M. Makihata, B. Liu, S. Zhou, Y.-h. Huang, H. Hu, Y. Gu, Y. Chen, Y. Lei, T. Lee, S. Chien, K.-I. Jang, E. B. Kistler, S. Xu, *Nat. Biomed. Eng.* **2021**, *5*, 749.
[18] G. R. Bashford, In V. B. Patel, V. R. Preedy, editors, *Biomarkers in Cardiovascular Disease*, Springer Science+Business Media, Berlin, Germany **2015**.
[19] C. Wang, X. Chen, L. Wang, M. Makihata, H.-C. Liu, T. Zhou, X. Zhao, *Science* **2022**, *377*, 517.
[20] W. D. O'Brien, *Radiographics: A Review Publication of the Radiological Society of North America, Inc* **1993**, *13*, 947.
[21] Q. Zhou, J. H. Cha, Y. Huang, R. Zhang, W. Cao, K. K. Shung, *IEEE Trans. Ultrason. Ferroelectr. Freq. Control* **2009**, *56*, 213.
[22] J. W. Hunt, M. Arditi, F. S. Foster, *IEEE Trans. Biomed. Eng.* **1983**, *BME-30*, 453.
[23] T.-G. La, L. H. Le, *Adva. Mater. Technol.* **2022**, *7*, 2100798.
[24] M. G. Grewe, T. Gururaja, T. R. Shrout, R. E. Newnham, *IEEE Trans. Ultrason. Ferroelectr. Freq. Control* **1990**, *37*, 506.
[25] M. State, P. J. Brands, F. N. van de Vosse, *Ultrasonics* **2010**, *50*, 458.
[26] A. Cafarelli, P. Miloro, A. Verbeni, M. Carbone, A. Menciassi, *J. Ultrasound* **2016**, *19*, 251.
[27] V. Genovés, M. D. Fariñas, R. Pérez-Aparicio, L. Saiz-Rodríguez, J. L. Valentín, T. G. Álvarez-Arenas, *Polymers* **2022**, *14*, 3614.
[28] S.-Y. Fu, X.-Q. Feng, B. Lauke, Y.-W. Mai, *Composites, Part B* **2008**, *39*, 933.
[29] J. Cho, M. Joshi, C. Sun, *Compos. Sci. Technol.* **2006**, *66*, 1941.
[30] R. Pal, *Composites, Part B* **2005**, *36*, 513.
[31] R. W. Style, R. Tutika, J. Y. Kim, M. D. Bartlett, *Adv. Funct. Mater.* **2021**, *31*, 2005804.
[32] R. W. Style, R. Boltyanskiy, B. Allen, K. E. Jensen, H. P. Foote, J. S. Wettlaufer, E. R. Dufresne, *Nat. Phys.* **2015**, *11*, 82.
[33] M. D. Bartlett, N. Kazem, M. J. Powell-Palm, X. Huang, W. Sun, J. A. Malen, C. Majidi, *Proc. Natl. Acad. Sci. U. S. A.* **2017**, *114*, 2143.
[34] E. J. Krings, H. Zhang, S. Sarin, J. E. Shield, S. Ryu, E. J. Markvicka, *Small* **2021**, *17*, 2104762.
[35] M. D. Bartlett, A. Fassler, N. Kazem, E. J. Markvicka, P. Mandal, C. Majidi, *Adv. Mater.* **2016**, *28*, 3726.
[36] M. H. Malakooti, N. Kazem, J. Yan, C. Pan, E. J. Markvicka, K. Matyjaszewski, C. Majidi, *Adv. Funct. Mater.* **2019**, *29*, 1906098.
[37] Y. Han, L.-E. Simonsen, M. H. Malakooti, *Adv. Energy Mater.* **2022**, *12*, 2201413.
[38] A. Haake, R. Tutika, G. M. Schloer, M. D. Bartlett, E. J. Markvicka, *Adv. Mater.* **2022**, *34*, 2200182.
[39] S. Liu, D. S. Shah, R. Kramer-Bottiglio, *Nat. Mater.* **2021**, *20*, 851.
[40] S. Kanetkar, N. U. H. Shah, R. M. Gandhi, A. Uppal, M. D. Dickey, R. Y. Wang, K. Rykaczewski, *ACS Appl. Eng. Mater.* **2023**, *1*, 1504.
[41] J. Wang, G. Cai, S. Li, D. Gao, J. Xiong, P. S. Lee, *Adv. Mater.* **2018**, *30*, 1706157.
[42] J. Tang, X. Zhao, J. Li, R. Guo, Y. Zhou, J. Liu, *ACS Appl. Mater. Interfaces* **2017**, *9*, 35977.
[43] C. J. Thrasher, Z. J. Farrell, N. J. Morris, C. L. Willey, C. E. Tabor, *Adv. Mater.* **2019**, *31*, 1903864.
[44] E. J. Markvicka, M. D. Bartlett, X. Huang, C. Majidi, *Nat. Mater.* **2018**, *17*, 618.
[45] M. J. Ford, C. P. Ambulo, T. A. Kent, E. J. Markvicka, C. Pan, J. Malen, T. H. Ware, C. Majidi, *Proc. Natl. Acad. Sci. U. S. A.* **2019**, *116*, 21438.
[46] P. Testa, R. W. Style, J. Cui, C. Donnelly, E. Borisova, P. M. Derlet, E. R. Dufresne, L. J. Heyderman, *Adv. Mater.* **2019**, *31*, 1900561.
[47] B. S. Chang, R. Tutika, J. Cutinho, S. Oyola-Reynoso, J. Chen, M. D. Bartlett, M. M. Thuo, *Mater. Horiz.* **2018**, *5*, 416.
[48] T. L. Buckner, M. C. Yuen, S. Y. Kim, R. Kramer-Bottiglio, *Adv. Funct. Mater.* **2019**, *29*, 1903368.
[49] S. Blairs, *Phys. Chem. Liq.* **2007**, *45*, 399.
[50] B. Yao, W. Hong, T. Chen, Z. Han, X. Xu, R. Hu, J. Hao, C. Li, H. Li, S. E. Perini, M. T. Lanagan, S. Zhang, Q. Wang, H. Wang, *Adv. Mater.* **2020**, *32*, 1907499.
[51] Y. Xu, Z. Lin, K. Rajavel, T. Zhao, P. Zhu, Y. Hu, R. Sun, C.-P. Wong, *Nano-micro Lett.* **2022**, *14*, 29.
[52] C. Y. Ho, S. D. Solomon, *Circulation* **2006**, *113*, e396.
[53] M. D. Dickey, R. C. Chiechi, R. J. Larsen, E. A. Weiss, D. A. Weitz, G. M. Whitesides, *Adv. Funct. Mater.* **2008**, *18*, 1097.
[54] R. C. Chiechi, E. A. Weiss, M. D. Dickey, G. M. Whitesides, *Angew. Chem., Int. Ed.* **2008**, *47*, 142.
[55] P. N. T. Wells, *Biomedical ultrasonics / P. N. T. Wells*, Medical physics series, Academic Press, London, **1977**.
[56] G. W. Willard, *J. Acoust. Soc. Am.* **2005**, *12*, 438.
[57] L. C. S. Nobre, A. F. Cristino, n. F. S. Santos, C. A. Nieto de Castro, I. M. S. Lampreia, *J. Chem. Thermodyn.* **2020**, *150*, 106226.
[58] C. Sayers, C. Tait, *Ultrasonics* **1984**, *22*, 57.

[59] I. D. Tevis, L. B. Newcomb, M. Thuo, *Langmuir* **2014**, *30*, 14308, pMID: 25372893.
[60] A. B. Wood, *A Textbook of Sound; Being an Account of the Physics of Vibrations with Special Reference to Recent Theoretical and Technical Developments*, Macmillan, New York, USA **1955**.
[61] F. Elias, J. Crassous, C. Derec, B. Dollet, W. Drenckhan, C. Gay, V. Leroy, C. Noûs, J. Pierre, A. Saint-Jalmes, *Curr. Opin. Colloid Interface Sci.* **2020**, *50*, 101391.
[62] W. Lee, H. Kim, I. Kang, H. Park, J. Jung, H. Lee, H. Park, J. S. Park, J. M. Yuk, S. Ryu, J.-W. Jeong, J. Kang, *Science* **2022**, *378*, 637.
[63] J. Souquet, P. Defranould, J. Desbois, *IEEE Trans. Son. Ultrason.* **1979**, *26*, 75.
[64] H. Ding, D. Yang, J. Xu, X. Chen, X. Le, Y. Wang, L. Lin, J. Xie, in *2020 IEEE 33rd Int. Conf. on Micro Electro Mechanical Systems (MEMS)*, IEEE, Piscataway, NJ **2020**, pp. 400.
[65] X. Xu, L. Sun, J. M. Cannata, J. T. Yen, K. K. Shung, *Ultrasound Med. Biol.* **2008**, *34*, 638.
[66] J. Yan, M. H. Malakooti, Z. Lu, Z. Wang, N. Kazem, C. Pan, M. R. Bockstaller, C. Majidi, K. Matyjaszewski, *Nat. Nanotechnol.* **2019**, *14*, 684.
[67] S. Everitt, V. Humphrey, *Ultrasonics* **2000**, *38*, 118.